

Fabrication and characterization of a nanostructured $\text{TiO}_2/\text{In}_2\text{S}_3\text{-Sb}_2\text{S}_3/\text{CuSCN}$ extremely thin absorber (eta) solar cell

This content has been downloaded from IOPscience. Please scroll down to see the full text.

2016 Semicond. Sci. Technol. 31 085011

(<http://iopscience.iop.org/0268-1242/31/8/085011>)

View [the table of contents for this issue](#), or go to the [journal homepage](#) for more

Download details:

IP Address: 148.234.94.150

This content was downloaded on 31/10/2016 at 22:48

Please note that [terms and conditions apply](#).

You may also be interested in:

[Elongated nanostructures for radial junction solar cells](#)

Yinghuan Kuang, Marcel Di Vece, Jatindra K Rath et al.

[Solution-processed \$\text{Cu}_2\text{ZnSnS}_4\$ superstrate solar cell using vertically aligned ZnO nanorods](#)

Dongwook Lee and Kijung Yong

[Fabrication of solution processed 3D nanostructured \$\text{CuInGaS}_2\$ thin film solar cells](#)

Van Ben Chu, Jin Woo Cho, Se Jin Park et al.

[Photovoltaic p-n structure of \$\text{MoSb}_2\text{xCu}_\text{x}\text{Se}_4/\text{CdS}\$ absorber films obtained via chemical bath deposition](#)

J J J Vijila, K Mohanraj and G Sivakumar

[Applications of atomic layer deposition in solar cells](#)

Wenbin Niu, Xianglin Li, Siva Krishna Karuturi et al.

[A review on plasma-assisted VLS synthesis of silicon nanowires and radial junction solar cells](#)

Soumyadeep Misra, Linwei Yu, Wanghua Chen et al.

[Antimony selenide thin film solar cells](#)

Kai Zeng, Ding-Jiang Xue and Jiang Tang

Fabrication and characterization of a nanostructured TiO₂/In₂S₃-Sb₂S₃/CuSCN extremely thin absorber (eta) solar cell

Alí M Huerta-Flores, Nora A García-Gómez,
Salomé M de la Parra-Arciniega and Eduardo M Sánchez

Universidad Autónoma de Nuevo León, UANL, Facultad de Ciencias Químicas, LabMat2:
Almacenamiento y Conversión de Energía, Av. Universidad S/N Ciudad Universitaria, San Nicolás de los
Garza, Nuevo León, C.P. 66455, México

E-mail: eduardo.sanchezcv@uanl.edu.mx

Received 30 January 2016, revised 28 April 2016

Accepted for publication 6 June 2016

Published 18 July 2016



CrossMark

Abstract

In this work we report the successful assembly and characterization of a TiO₂/In₂S₃-Sb₂S₃/CuSCN extremely thin absorber solar cell. Nanostructured TiO₂ deposited by screen printing on an ITO substrate was used as an n-type electrode. An ~80 nm extremely thin layer of the system In₂S₃-Sb₂S₃ deposited by successive ionic layer adsorption and a reaction (silar) method was used as an absorber. The voids were filled with p-type CuSCN and the entire assembly was completed with a gold contact. The solar cell fabricated with this heterostructure showed an energy conversion efficiency of 4.9%, which is a promising result in the development of low cost and simple fabrication of solar cells.

Keywords: extremely thin absorber solar cell, In₂S₃, Sb₂S₃, silar

(Some figures may appear in colour only in the online journal)

1. Introduction

One of the greatest challenges humanity is facing is the development of technologies based on renewable energies. Over recent years, attention has been focused on solar energy, where the final goal is the fabrication of low cost and high performance photovoltaic devices [1]. The concept of an extremely thin absorber (eta) solar cell has emerged with great expectations, due to the numerous advantages given by this novel design. The eta solar cell is a photovoltaic device of 2 to 10 μm of thickness, made of an extremely thin absorber material forming an interpenetrating heterogeneous junction with p-type material and n-type material [2]. This design combines the advantages of using an extremely thin absorber material of cheap and easy preparation deposited on nanostructured substrates with the characteristic stability of solid state solar cells [3]. Besides, the optical scattering on the surface of the nanostructured substrate will enhance the optical path of the light inside the absorber material, promoting better photon absorption. This effect is known as light

trapping [4]. Due to this design, the use of materials with low electronic quality becomes possible, therefore, low cost materials can be used as absorbers.

Different chalcogenides have been widely studied as possible absorber materials in photovoltaic devices: PbSe [5], CdSe [6], Sb₂Se₃ [7], CdTe [8], CdS [9], PbS [10], In₂S₃ [11], Cu_{2-x}S [12], CuInS₂ [13], and Sb₂S₃ [14]. Solar cells constructed with indium [11] and antimony [14] sulphides have showed promising conversion efficiencies: 2.3% and 3.7%, respectively. Both sulphides are very attractive materials due to their stability and remarkable optical properties, such as suitable band gaps for absorber layers (E_g In₂S₃ = 2.1 eV and E_g Sb₂S₃ = 1.8 eV) and high absorption coefficients.

As a window layer and n-type material TiO₂ (E_g = 3.15 eV) [15] and ZnO (3.35 eV) [16] have been extensively used. The unique properties of charge transport and low recombination rates observed on TiO₂ contributed to make this material the most suitable n-type semiconductor for solar cells. CuSCN (E_g = 3.60 eV) [17] and PEDOT:PPS (E_g = 1.40–2.5 eV) [18] have been commonly studied as

p-type materials. High efficiencies have been obtained with heterostructures conformed by TiO₂ and CuSCN as n and p-type materials [19–22]. The use of a nanostructured substrate of n-type material on an eta solar cell increases the optical path of light inside the structure and promotes a better absorption. For instance, TiO₂ thin layers have been deposited by spin coating [23] and dip coating [24] techniques, through precursors prepared by sol–gel methodologies: electrostatic-

layer-by-layer deposition is also used for making TiO₂ films. It combines both the sol–gel and block copolymers for the synthesis of TiO₂ films [25]. These techniques involve the deposition *in situ* of TiO₂ thin layers by the process of hydrolysis and condensation from a precursor solution (metallic salts or alcoxides) on the substrate, followed by a heat treatment, this will conduce to the preparation of thin layers with dense nanocrystalline structure or macropores [23] of limited porosity for its application on solar cells. The addition of block copolymers on the precursor solution is a good alternative to improve the mesoporosity, leading to the obtention of ordered mesopores on the layer and an increase on the surface area [26]. Techniques involving the use of block copolymers are screen printing [27] and doctor blades [28].

Electrochemical [29], vapor phase epitaxial [16] and ionic layer gas reaction [13] deposition methods, among others, have been used in the preparation of thin layers of absorber materials for solar cells. Recently, successive ionic layer adsorption and the reaction (silar) method has been used for the deposition of CdS and CdTe thin layers for eta solar cells [30]. This method involves an effective mechanism for the deposition of thin and homogeneous layers, and consists of the immersion of the substrate in a sequential order in two separate solutions: a cationic and an anionic solution with an intermediate rising stage. The advantages of this method include its simplicity, the capacity to carry the process at room temperature through simple cationic and anionic precursors and the controlled and uniform growth of the layers. The thickness of the deposited layers can be controlled by the

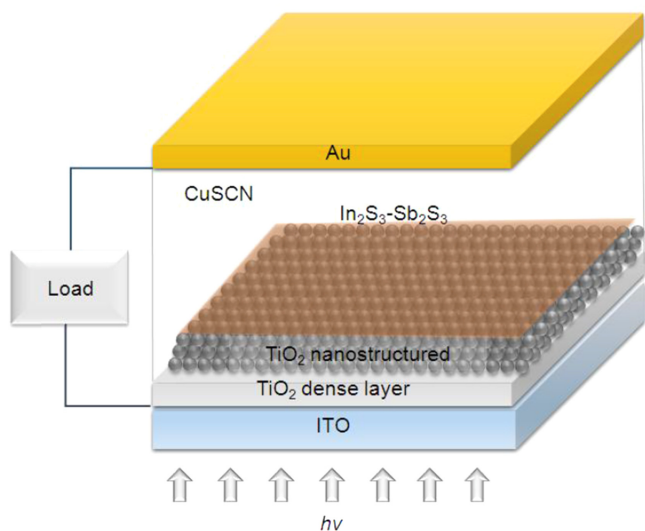


Figure 1. General construcción of a TiO₂/In₂S₃-Sb₂S₃/CuSCN solar cell.

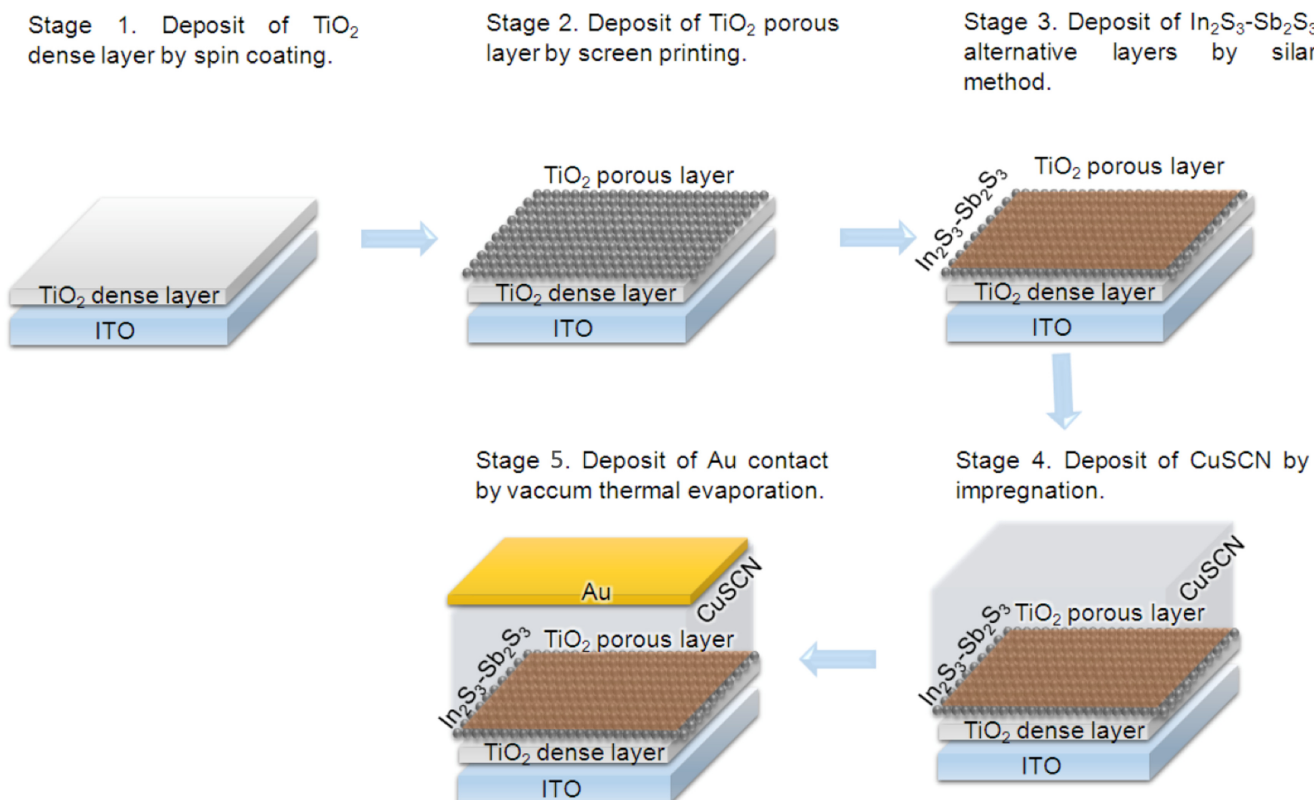


Figure 2. Illustration of the fabrication process of a TiO₂/In₂S₃-Sb₂S₃/CuSCN extremely thin absorber solar cell.

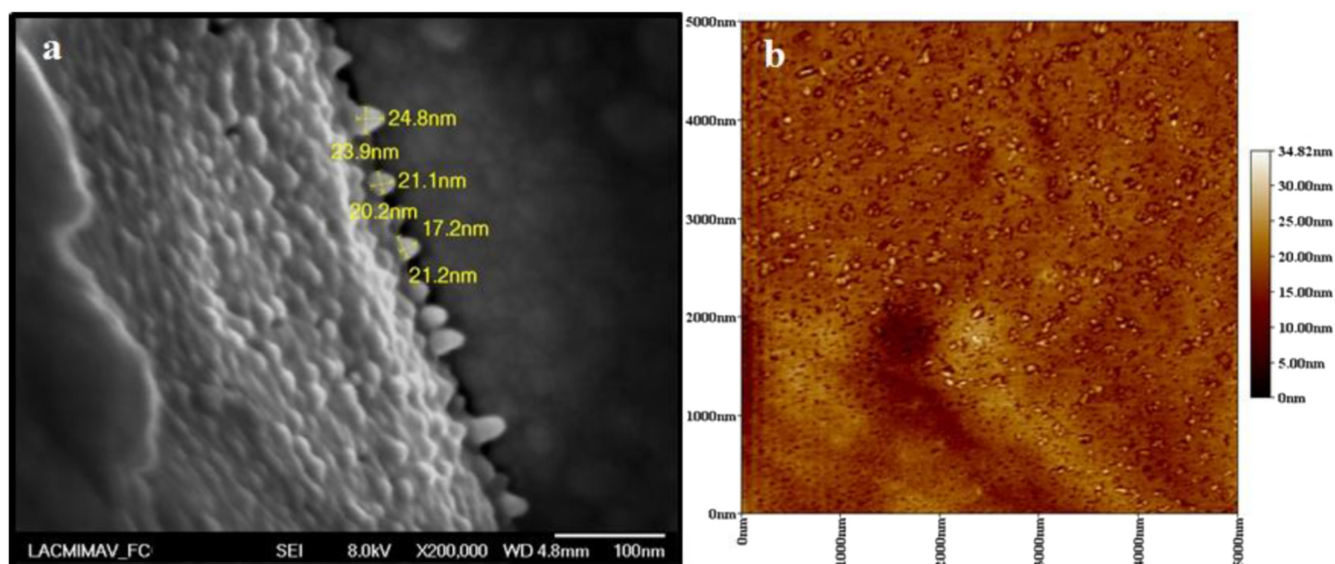


Figure 3. (a) SEM and (b) AFM images of a TiO₂ dense layer deposited by spin coating on conducting glass.

number of deposition cycles. In this work we study the heterostructure TiO₂/In₂S₃-Sb₂S₃/CuSCN on eta solar cells. In order to enhance the capacity of light absorption of the solar cell and improve its efficiency, alternative layers of In₂S₃-Sb₂S₃ were deposited by the silar method over a nanostructured substrate of TiO₂. A p-type material and hole transporter CuSCN is used.

2. Experimental

The heterostructure of the constructed eta solar cell and its band diagram is shown in figure 1. Commercial indium-tin oxide (ITO) conducting glass (10 W cm⁻²) was used as substrates. The substrates were rinsed ultrasonically in acetone, isopropanol and deionized water for 15 min before deposition. In order to avoid a short circuit between the p-type semiconductor and the substrate, a TiO₂ seed layer was grown on coated glass by the spin-coating method. The TiO₂ precursor solution was prepared dissolving 3 ml of titanium isopropoxide (C₁₂H₂₈O₄Ti, 97% Aldrich) and 2 ml of diethanolamine (C₄H₁₁NO₂, 98% Sigma-Aldrich) in 10 ml of absolute ethanol (Fermont). The solution was stirred for 10 min. The deposition was carried out using a laboratory-made spin-coater, adding 1 ml of TiO₂ precursor solution on the conductive side of the substrate and rotating at 1000 rpm for 2 min. The deposited TiO₂ thin layer was annealed for 30 min at 450 °C.

For the n-type material, a nanostructured porous TiO₂ layer was deposited over the seed layer by a screen printing method. The paste used for the deposition was prepared by grinding 10 g of TiO₂ (P25 Degussa) with 20 ml of absolute ethanol and 1 ml of acetic acid (CH₃COOH, CTR Scientific). The paste was dispersed in an ultrasonic bath for 2 min. The screen printing deposition was carried out through a polyester mesh (60 mm). The TiO₂ porous layer was annealed for 60 min at 450 °C.

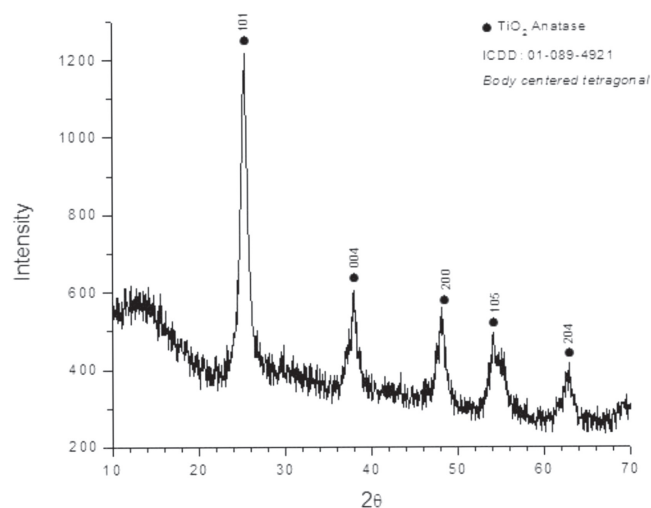


Figure 4. XRD pattern of a TiO₂ dense layer deposited by spin coating.

In₂S₃ and Sb₂S₃ thin layers were deposited over the TiO₂ porous layer by the silar method. The precursors used were antimony (III) chloride (SbCl₃, 99% Sigma-Aldrich), indium (III) chloride (InCl₃, 99% Sigma-Aldrich), 99% Sigma-Aldrich) and thioacetamide (C₂H₅NS, 95% Sigma Aldrich). A 0.2 M metal sulphide solution in ethanol was used as cationic solution, and 0.3 M thioacetamide in ethanol as anionic precursor. The substrate was immersed for 5 min on the cationic precursor, rinsed with deionized water and then immersed for 5 min on the anionic precursor with a final step of rinsing with deionized water. The thin layer deposited was annealed on a vacuum oven (Shel Lab 1410, 3 × 10⁻³ torr) for 30 min at 150 °C, and then a second layer of the alternative system was deposited using the same procedure. Five deposition cycles of the system In₂S₃-Sb₂S₃ were used for the preparation of the absorber layer.

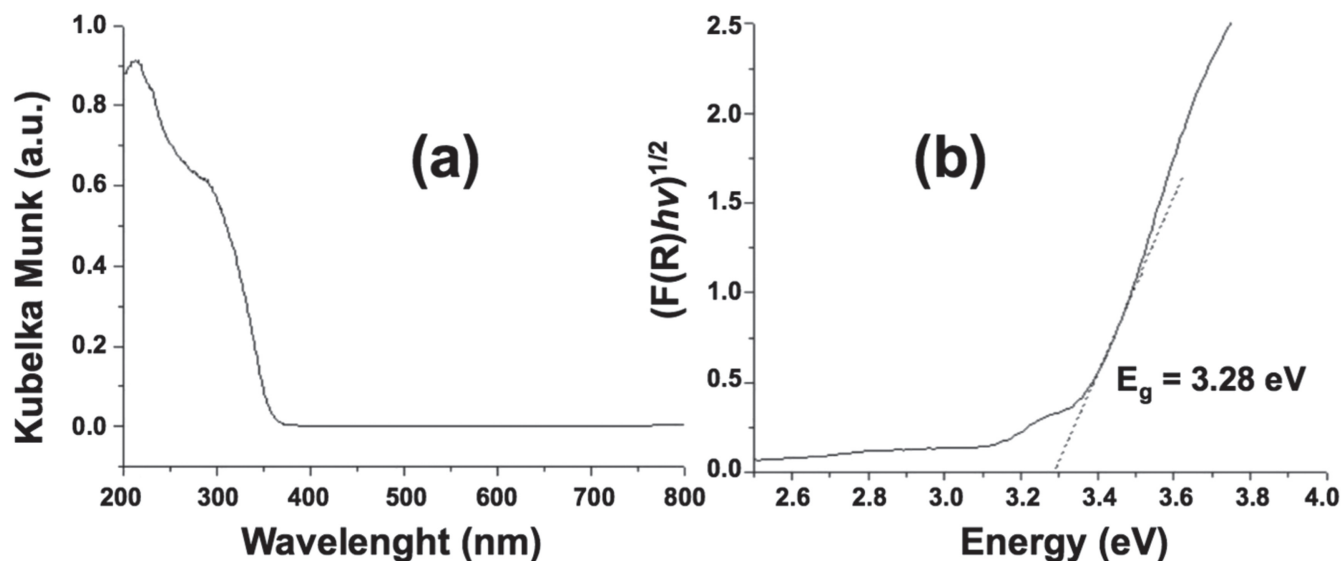


Figure 5. (a) Reflectance spectra of a TiO₂ dense layer deposited by spin coating, and (b) calculated Tauc plot.

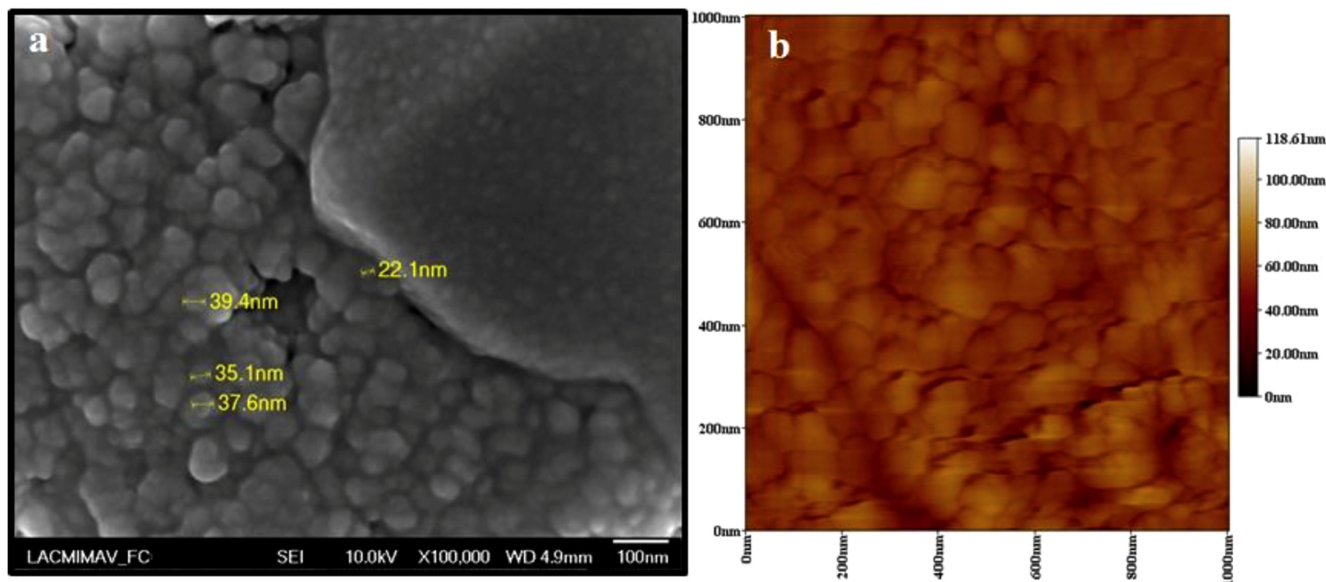


Figure 6. (a) SEM and (b) AFM images of a TiO₂ porous layer deposited by screen printing.

For the p-type material, a thin layer of CuSCN was deposited by an impregnation method over the absorber material. A saturated solution of CuSCN in propyl sulphide was required. 0.5 ml of the saturated solution was dropped on the substrate pre-heated at 80 °C. The deposited layer was annealed 30 min at 250 °C. For the negative electrode, a nanostructured substrate of TiO₂ covered with the absorber system and a p-type material was used, and for the positive electrode, a gold contact was deposited by vacuum thermal evaporation. Figure 2 shows the entire process of fabrication of the TiO₂/In₂S₃-Sb₂S₃/CuSCN extremely thin absorber solar cell.

The structural properties of the prepared thin films were analyzed by x-ray diffraction, using a Bruker D8 Advance

diffractometer operating at 40 kV and 40 mA with Cu K α radiation ($\lambda = 1.5406 \text{ \AA}$), from 10° to 70° (2θ angle). The scanning electron microscopy images were recorded on a JEOL Model JCM-6000. Surface rugosity was studied through a Nanoscope III Multimode AFM. Optical properties were analyzed using a UV-vis spectrophotometer (Nicolet Evolution 300 PC) in the diffuse reflectance mode. Current-voltage (I - V) measurements was performed on a potentiostat-galvanostat Metrohm Autolab, using a Xenon lamp of 150 W as the white light source; the intensity of the lamp was measured through a piranometer (Eplab spectral). The solar cell was illuminated with an intensity of 500 W m⁻² at AM 1.5 and 25 °C. The effective area of the solar cell was 1.5 cm².

3. Results and discussion

SEM and AFM images of the TiO₂ dense layer deposited by spin coating are shown in figure 3. As can be seen in figure 3(a), the TiO₂ dense layer shows a uniform deposit of particles with a grain size around 20 nm. The rugosity observed in figure 3(b) was around 34.82 nm. According to this, the TiO₂ dense layer showed a low rugosity as expected for a dense layer, and an homogeneous coverage over the conducting substrate, so it will be functional as a seed layer for the deposition of a porous layer and for avoiding the contact between the p-type material and conducting glass. Figure 4 shows the XRD pattern of the prepared TiO₂ dense layer. As shown on figure 4, the TiO₂ dense layer exhibits the characteristic diffraction peaks of the anatase phase (ICDD: 01-089-4921) of a body-centered tetragonal structure.

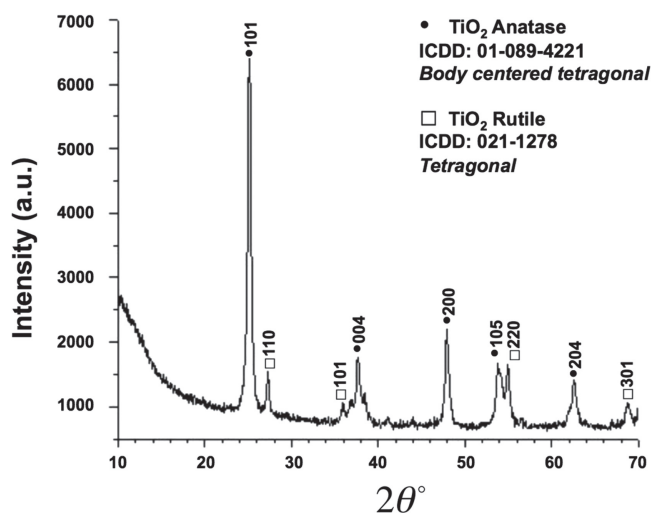


Figure 7. XRD pattern of the TiO₂ porous layer deposited by screen printing.

The production of the anatase phase was favored by the annealing treatment employed (450 °C-60 min) and the sol-gel method.

The diffuse reflectance spectra of the TiO₂ dense layer were obtained by UV-vis spectroscopy. Figure 5(a) shows the reflectance spectra of the TiO₂ dense layer deposited by spin coating and figure 5(b) shows the calculated Tauc plot. As shown in figure 5(a), the obtained reflectance spectra corresponds to TiO₂, considering this compound absorbs energy on lower wavelengths, to 400 nm. The band gap of the TiO₂ layer was calculated through the Tauc plot shown in figure 5(b), using a value of n equal to $\frac{1}{2}$ due to TiO₂ exhibiting indirect transitions [31]. The calculated band gap was 3.28 eV, which corresponds to TiO₂. The morphology and crystalline structure SEM and AFM images of the TiO₂ porous layer deposited by screen printing are shown in figure 6. As can be seen in figure 6(a), the TiO₂ porous layer shows a deposit of a rough layer with a homogeneous particle distribution. The observed grains showed an average size of 37 nm. The rugosity observed in figure 6(b) was around 118.61 nm. The AFM image shows the deposit of the TiO₂ porous layer with uniform morphology and particles of uniform size. The high rugosity presented by the TiO₂ porous layer is favorable because it will work as a nanostructured substrate on the solar cell and promote a larger optical path of light inside the structure and better photon absorption. Figure 7 shows the XRD pattern of the prepared TiO₂ porous layer. As shown in figure 7, the TiO₂ porous layer exhibits two phases, the first being the principal phase anatase (ICDD: 01-089-4921) of body-centered tetragonal structure, and the secondary phase, rutile, (ICDD: 021-1276) of tetragonal structure. The presence of a rutile phase is attributed to the TiO₂ nanoparticles used for the preparation of the screen printing paste (P25 Degussa), which present both phases in their composition. For photovoltaic applications, anatase is considered the most active phase of TiO₂, as this phase

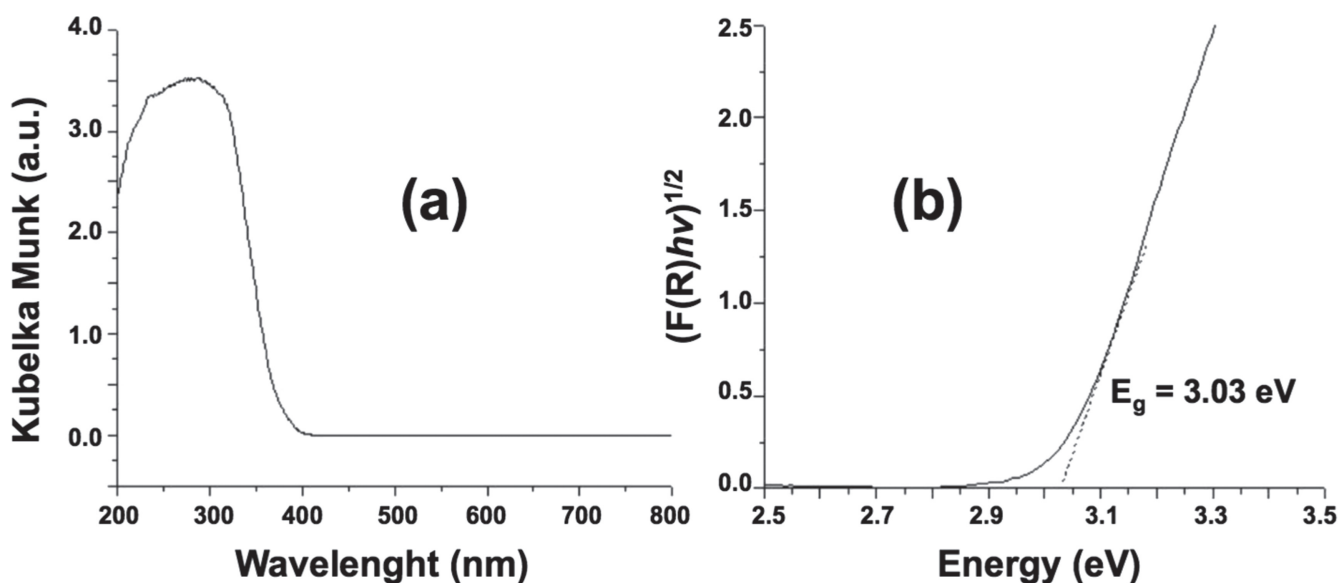


Figure 8. (a) Reflectance spectra of the TiO₂ porous layer deposited by screen printing, and (b) calculated Tauc plot.

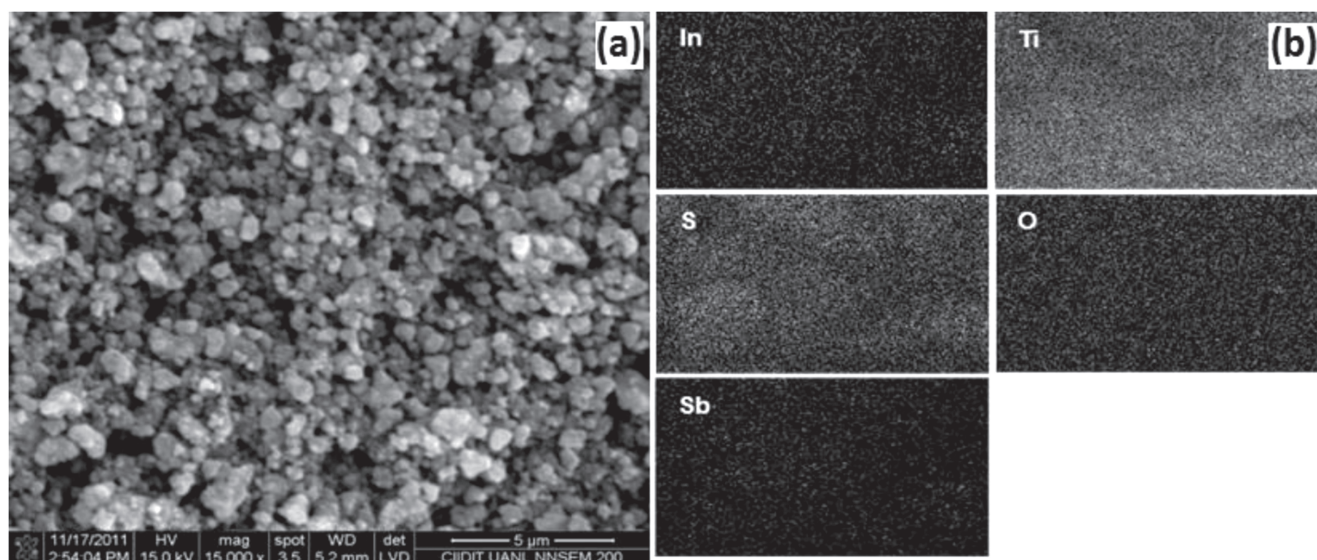


Figure 9. (a) SEM image of the $\text{In}_2\text{S}_3\text{-Sb}_2\text{S}_3$ absorber layer deposited by the silar method on a TiO_2 nanostructured substrate, and (b) elemental mapping made by EDS.

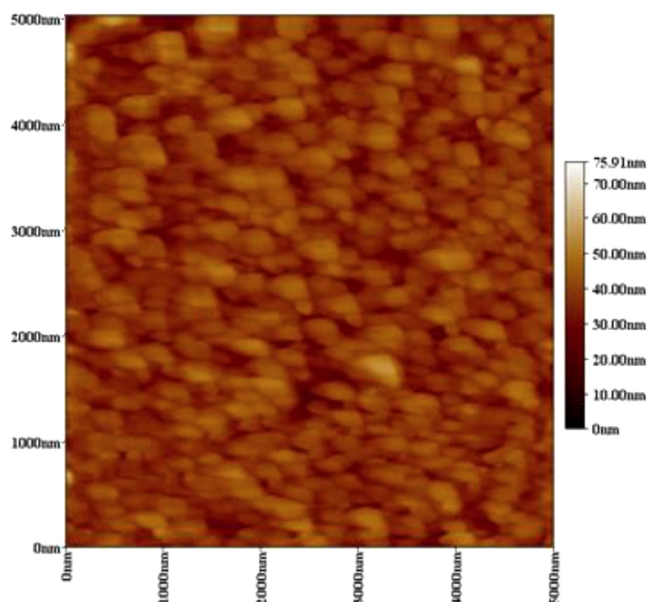


Figure 10. AFM image of the $\text{In}_2\text{S}_3\text{-Sb}_2\text{S}_3$ absorber layer deposited by the silar method.

presents a high superficial area, given by its crystallographic orientation and its higher band gap energy. On rutile, the recombination process occurs more frequently, which is detrimental for the efficiency of solar cells [32].

The diffuse reflectance spectra of the TiO_2 porous layer was obtained by UV-vis spectroscopy. Figure 8(a) shows the reflectance spectra of TiO_2 porous layer deposited by screen printing and figure 8(b) shows the calculated Tauc plot. As shown in figure 8(a), the obtained reflectance spectra of the TiO_2 porous layer corresponds, as does the TiO_2 dense layer, to TiO_2 , showing absorption on the ultraviolet region. The band gap energy of the TiO_2 porous layer was calculated

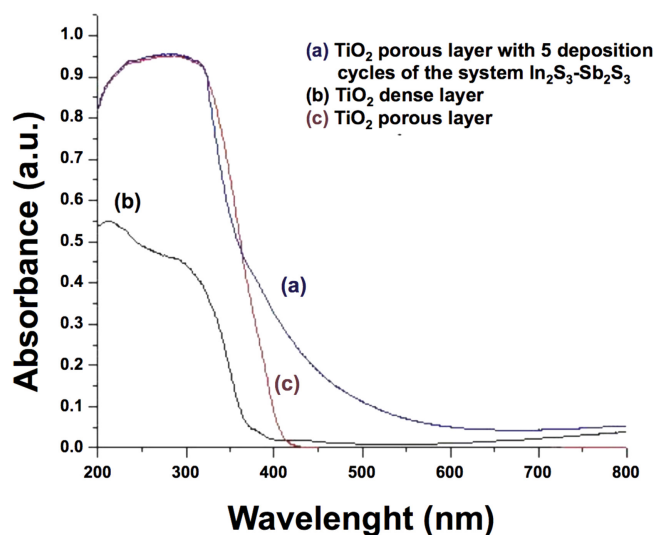


Figure 11. (a) Absorbance spectra of the $\text{In}_2\text{S}_3\text{-Sb}_2\text{S}_3$ absorber layer compared to that obtained by TiO_2 (b) dense and (c) porous layer.

through the Tauc plot shown in figure 8(b), using the same procedure described before. The decrease of the band gap energy can be attributed to the presence of the rutile phase. The band gap energy reported for anatase is 3.20 eV [33], while for the rutile phase is 3.02 eV [33]. Figure 9(a) shows the morphology of the $\text{In}_2\text{S}_3\text{-Sb}_2\text{S}_3$ absorber layer deposited by the silar method and figure 9(b) shows the elemental mapping made by energy dispersive x-ray spectroscopy (EDS). As can be seen in figure 9(a), the $\text{In}_2\text{S}_3\text{-Sb}_2\text{S}_3$ absorber layer presents a homogeneous and rough surface with particles of regular size. This morphology is similar to that observed on the TiO_2 nanostructured substrate, so we assume that the deposition of the absorber layer did not modify the morphology of the nanostructured TiO_2 . The

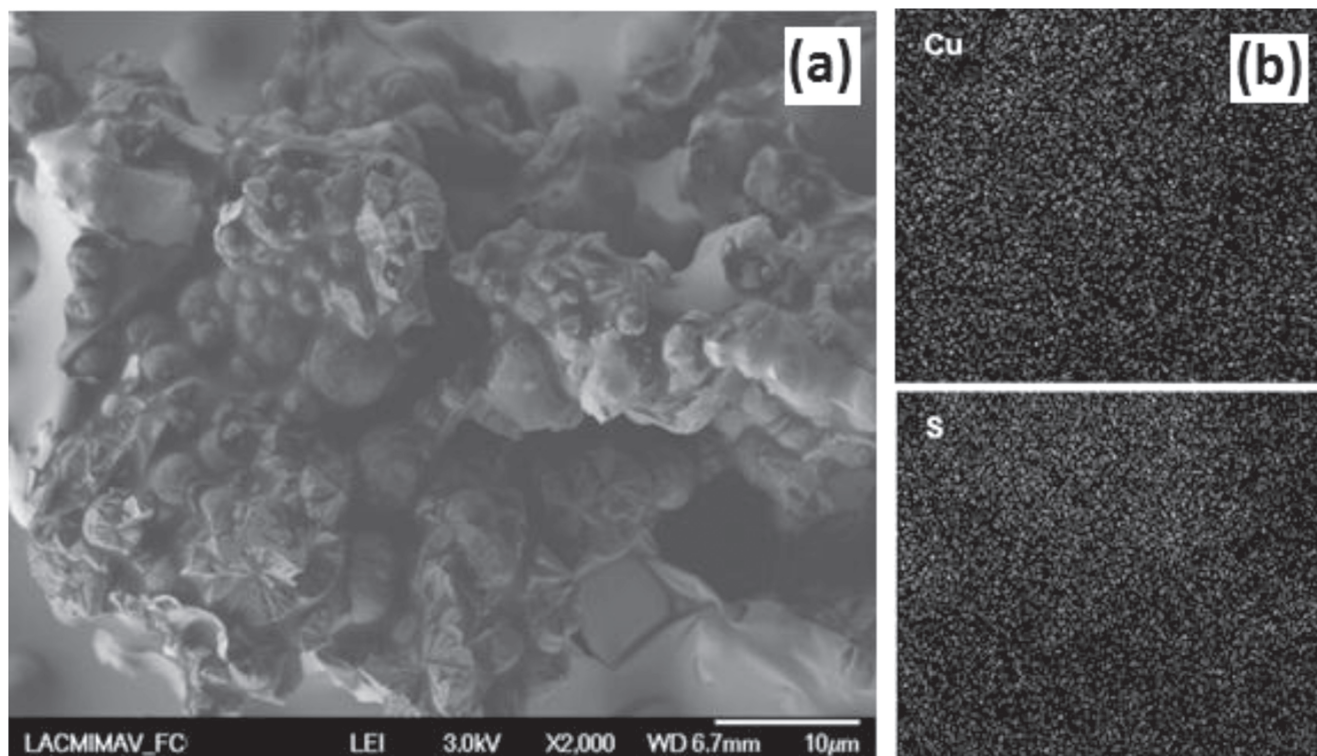


Figure 12. (a) SEM image of the CuSCN layer deposited by impregnation, and (b) elemental mapping made by EDS.

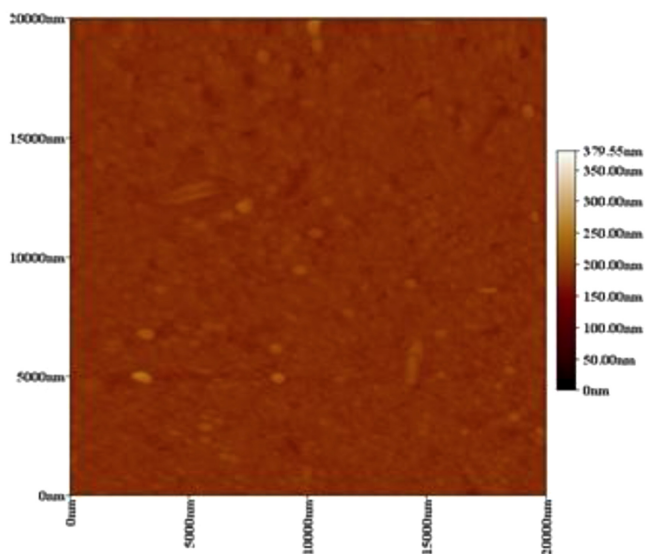


Figure 13. AFM image of the CuSCN layer deposited by impregnation.

elemental mapping carried out by EDS confirmed the deposition of the absorber material on the TiO₂ substrate and the homogeneity of the deposit. Figure 10 shows the AFM image of the In₂S₃-Sb₂S₃ absorber layered by the silar method. As shown in figure 10, the roughness observed on the In₂S₃-Sb₂S₃ absorber layer was around 75.91 nm, which confirms the formation of an extremely thin absorber layer (<100 nm). The image obtained by AFM of the absorber layer showed the deposit of a thin layer with a homogeneous

surface and particles of regular size. Figure 11 shows the XRD pattern obtained by the In₂S₃-Sb₂S₃ absorber layer deposited by the silar method on the TiO₂ nanostructured substrate. The XRD pattern of the In₂S₃-Sb₂S₃ absorber layer on TiO₂ nanostructured substrate exhibits two phases, one being the principal anatase with a body-centered tetragonal structure, and the secondary phase, rutile, of tetragonal structure, which is quite similar to the TiO₂ porous layer in figure 7. No additional peaks were observed on the XRD pattern. This can be possibly attributed by two reasons: 1) the absorber layer presents low crystallinity or 2) the amount of absorber material deposited is too small to be detected by this technique. The confirmation of the deposit of the absorber layer was carried out by EDS, as shown in figure 9(b).

The absorbance spectra of the In₂S₃-Sb₂S₃ absorber layer deposited by the silar method on TiO₂ nanostructured substrate is shown in figure 11(a), compared to that obtained by the TiO₂ dense (figure 11(b)) and porous (figure 11(b)) layer. As shown in figure 11, the absorbance of the TiO₂ porous layer is modified by the deposit of the In₂S₃-Sb₂S₃ absorber layer, showing an increase of the absorbance on the visible region of the spectrum. This result confirms the fact the absorber layer is harvesting the light on the visible region of the spectrum due to the characteristic absorption properties of In₂S₃ and Sb₂S₃. Figure 12(a) shows the morphology of the CuSCN layer deposited by impregnation and figure 12(b) shows the elemental mapping made by EDS. As can be seen in figure 13(a), the CuSCN layer presents a rough surface with particles of regular size.

Elemental mapping confirms the uniform deposit of CuSCN over the absorber material. Figure 13 shows an AFM image of the CuSCN layer deposited by impregnation. As shown in figure 13, the roughness observed on the CuSCN layer was around 379.55 nm. The image obtained by AFM shows a surface of homogeneous morphology and particles of uniform size. Figure 14 shows the XRD pattern obtained by the In_2S_3 CuSCN layer deposited by impregnation. As shown in figure 14, the XRD pattern of the CuSCN layer exhibits the characteristic peaks of the phase β -CuSCN (ICDD: 029-0581) of rhombohedral structure. The diffuse reflectance spectrum of the CuSCN layer was obtained by UV-vis spectroscopy. Figure 15(a) shows the reflectance spectra of CuSCN and figure 16(b) shows the calculated Tauc plot. As shown in figure 15(a), the obtained spectra correspond to CuSCN, as this

compound absorbs energy to wavelengths to 350 nm. The band gap energy was calculated through the Tauc plot showed in figure 15(b), using a value of n equal to 2 due to CuSCN presenting direct transitions [34]. The calculated band gap was of 3.67 eV, which corresponds to that reported for CuSCN [17].

As we described in section 2, the electrical characterization of the device was performed illuminating the solar cell with an intensity of 500 W m^{-2} at AM 1.5 and 25°C . The effective area of the solar cell was 1.5 cm^2 . In order to study the effect of the addition of both systems as absorber layers (In_2S_3 - Sb_2S_3), additional eta solar cells were prepared using only In_2S_3 or Sb_2S_3 as absorber materials. Three solar cells were characterized, we show, in figure 16, the most representative I - V curves. The characteristic parameters of the solar cells, the short circuit current density (J_{sc}), open circuit voltage (V_{oc}), fill factor (FF) and conversion efficiency were extracted from the data shown in figure 16 and have been summarized in table 1. The total efficiency obtained from the eta solar cell assembled in this work was higher than that obtained by the solar cells using absorber materials as separate sulphides. This could be attributed to the effective band alignment of the materials on the heterostructure, a better light absorption due to the combination of the absorption properties of each sulphide and, probably, to the realization of reduced thickness of the absorber material through a better control of the deposition layers by the silar method.

In figure 17 we present an energy level diagram of the $\text{ITO}/\text{TiO}_2/\text{In}_2\text{S}_3\text{-Sb}_2\text{S}_3/\text{CuSCN}/\text{Au}$ solar cell. The conduction band (CB) and valence band (VB) edges were obtained from the literature [35] where we can see the alignment at the interface of the heterostructure. As can be seen, In_2S_3 and Sb_2S_3 CBs and VBs are in a favorable position with respect to the TiO_2 and CuSCN layers, so the photons will be absorbed on the $\text{In}_2\text{S}_3\text{-Sb}_2\text{S}_3$ layers and the electrons will be promoted to the TiO_2 layer, while holes will be transported to the

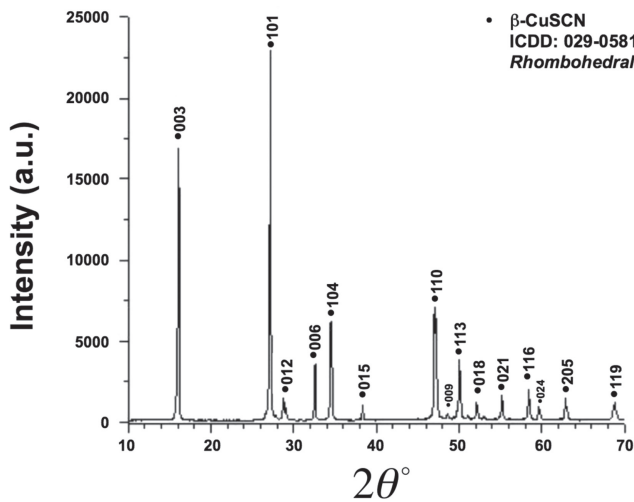


Figure 14. XRD pattern of the CuSCN layer deposited by impregnation.

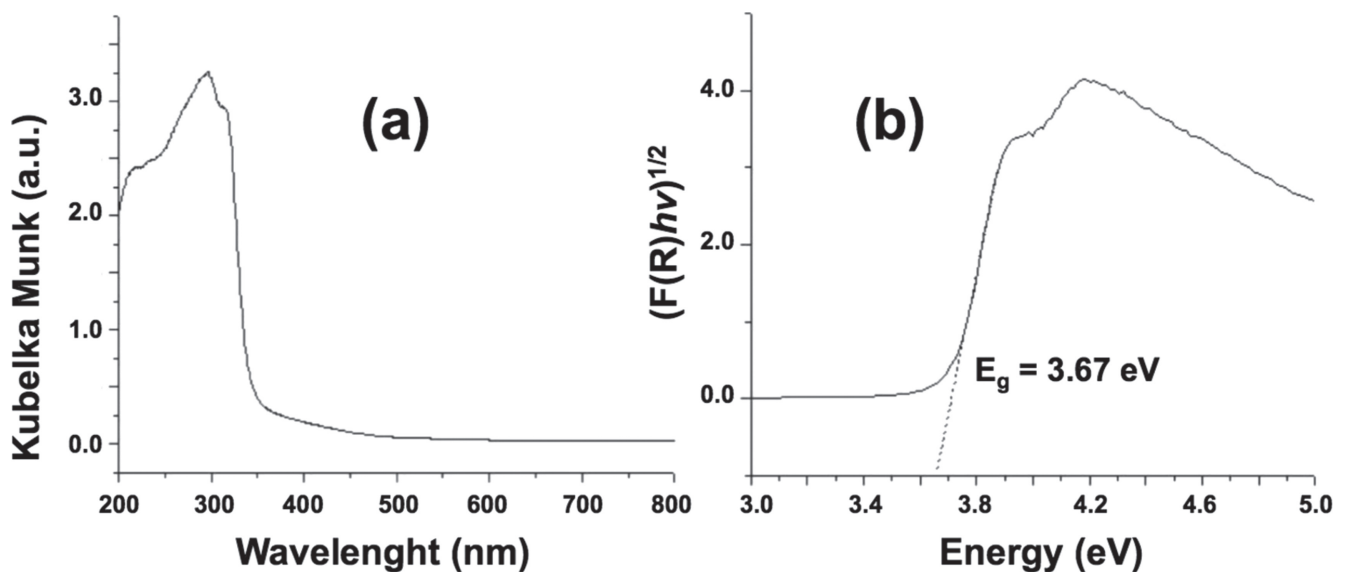


Figure 15. (a) Reflectance spectra of the CuSCN layer deposited by impregnation, and (b) calculated Tauc plot.

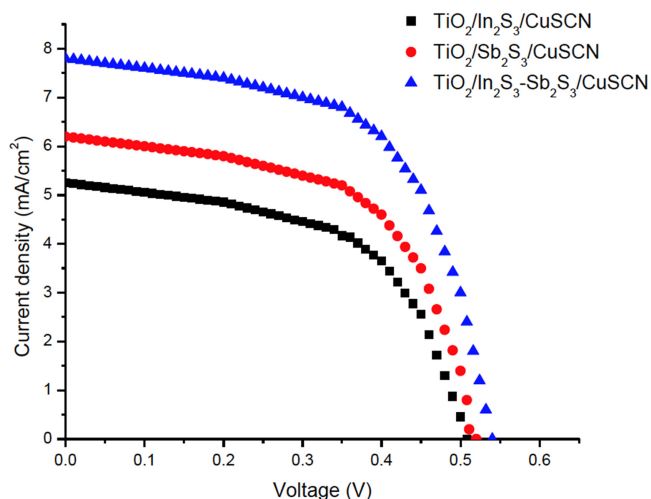


Figure 16. *J-V* curve of nanostructured eta solar cells under illuminated conditions (500 W m^{-2} , AM 1.5, $T = 25 \text{ }^\circ\text{C}$).

CuSCN layer. According to this, $\text{In}_2\text{S}_3\text{-Sb}_2\text{S}_3$ is a good candidate to act as an absorber layer.

4. Conclusions

We have demonstrated the fabrication and characterization of a nanostructured $\text{TiO}_2/\text{In}_2\text{S}_3\text{-Sb}_2\text{S}_3/\text{CuSCN}$ extremely thin absorber solar cell. The heterostructure showed a promising efficiency conversion of 4.9%, which indicates that it has a favorable band alignment and good photon harvesting on the visible region of the spectrum. This led to the formation of higher efficiencies than sulphides as absorber materials by separation. This solar cell design provides a good alternative photovoltaic device fabricated from relatively non-toxic and abundant materials through simple and cheap preparation methods.

Table 1. Characteristic parameters of eta solar cells obtained by illuminating the cells at 500 W m^{-2} , AM 1.5, $T = 25 \text{ }^\circ\text{C}$.

Structure of the eta solar cell	V_{oc} (V)	J_{sc} (mA cm^{-2})	FF	Efficiency (%)
$\text{TiO}_2/\text{In}_2\text{S}_3\text{-Sb}_2\text{S}_3/\text{CuSCN}$	0.545	7.8	0.58	4.9
$\text{TiO}_2/\text{In}_2\text{S}_3/\text{CuSCN}$	0.508	5.2	0.55	2.9
$\text{TiO}_2/\text{Sb}_2\text{S}_3/\text{CuSCN}$	0.520	6.2	0.56	3.6

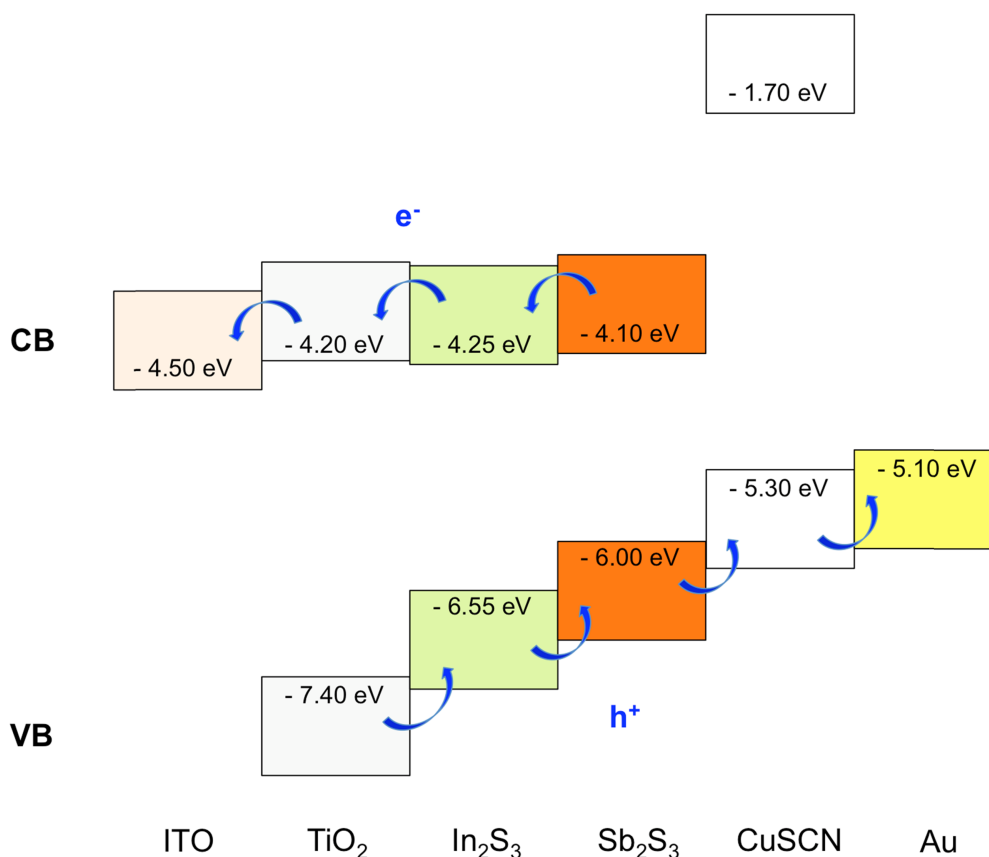


Figure 17. Energy level diagram of a $\text{TiO}_2/\text{In}_2\text{S}_3\text{-Sb}_2\text{S}_3/\text{CuSCN}$ solar cell.

Acknowledgments

The authors would like to thank the Universidad Autónoma de Nuevo León and SENER-CONACYT for financially supporting this research under research projects 150111 and 256766.

References

- [1] Graetzel M, Janssen R A, Mitzi D B and Sargent E H 2012 Materials interface engineering for solution-processed photovoltaics *Nature* **488** 304
- [2] Ernst K, Belaidi A and Könenkamp R 2003 Solar cell with extremely thin absorber on highly structured substrate *Semicond. Sci. Tech.* **18** 475
- [3] Dittrich T, Belaidi A and Ennaoui A 2011 Concepts of inorganic solid-state nanostructured solar cells *Sol. Energ. Mat. Sol. C* **95** 1527
- [4] Briscoe J and Dunn S 2011 Extremely thin absorber solar cells based on nanostructured semiconductors *Energ. Mat.* **6** 1741
- [5] Choi J J et al 2009 PbSe nanocrystal excitonic solar cells *Nano Lett.* **9** 3749
- [6] Lévy-Clément C, Tena-Zaera R, Ryan M A, Katty A and Hodes G 2005 CdSe-sensitized p-CuSCN/nanowire n-ZnO heterojunctions *Adv. Mat.* **17** 1512
- [7] Ngo T T, Chavhan S, Kosta I, Miguel O, Grande H J and Tena-Zaera R 2014 Electrodeposition of antimony selenide thin films and application in semiconductor sensitized solar cells *ACS Appl. Mater. Interfaces* **6** 2836
- [8] Tena-Zaera T, Katty A, Bastide S, Lévy-Clément C, O'Regan B and Muñoz-Sanjose V 2005 ZnO/CdTe/CuSCN, a promising heterostructure to act as inorganic eta-solar cell *Thin Solid Films* **483** 372
- [9] Larramona G, Chone C, Jacob A, Sakakura D, Delatouche B, Peré D, Cieren X, Nagino M and Bayón R 2006 Nanostructured photovoltaic cell of the type Titanium dioxide, cadmium sulfide thin coating, and copper thiocyanate showing high quantum efficiency *Chem. Mater.* **18** 1688
- [10] Biancardo M and Krebs F C 2007 Microstructured extremely thin absorber solar cells *Sol. Energ. Mat. Sol. C* **91** 1755
- [11] Herzog C, Belaidi A, Ogacho A and Dittrich T 2009 Inorganic solid state solar cell with ultra-thin nanocomposite absorber based on nanoporous TiO₂ and In₂S₃ *Eng. Environ. Science* **2** 962
- [12] Page M, Niitsoo O, Itzhaik Y, Cahen D and Hodes G 2009 Copper sulfide as a light absorber in wet-chemical synthesized extremely thin absorber (ETA) solar cells *Eng. Environ. Science* **2** 220
- [13] Kaiser I, Ernst K, Fischer C H, Könenkamp R, Rost C, Sieber I and Steiner M C 2001 The eta-solar cell with CuInS₂: a photovoltaic cell concept using an extremely thin absorber (eta) *Sol. Energ. Mat. Sol. C* **67** 89
- [14] Nezu S, Larramona G, Chone C, Jacob A, Delatouche B, Pere D and Moisan C 2010 Light soaking and gas effect on nanocrystalline TiO₂/Sb₂S₃/CuSCN photovoltaic cells following extremely thin absorber concept *J. Phys. Chem. C* **114** 6854
- [15] Könenkamp R, Hoyer P and Wahi A 1996 Heterojunctions and devices of colloidal semiconductor films and quantum dots *J. Appl. Phys.* **79** 7029
- [16] Lévy-Clément C, Katty A, Bastide S, Zenia F, Mora I and Muñoz Sanjose V 2002 A new CdTe/ZnO columnar composite film for eta-solar cells *Physica E* **14** 229
- [17] Tennakone K, Kumara G R R A, Kottegoda I R M, Perera V P S and Aponso G M L P 1998 Nanoporous n-TiO₂/selenium/p-CuSCN photovoltaic cell *J. Phys. D: Appl. Phys.* **31** 2326
- [18] Groenendaal L, Jonas F, Freitag D, Pielartzik H and Reynolds J R 2000 Poly(3,4-ethylenedioxythiophene) and Its derivatives: past, present, and future *Adv. Mater.* **12** 481
- [19] Muto T, Larramona G and Dennler G 2013 Unexpected performances of flat Sb₂S₃-based hybrid extremely thin absorber solar cells *Appl. Phys. Express* **6** 072301
- [20] We Y, Assaud L, Kryschi C, Capon B, Detavernier C, Santinacci L and Bachmann J 2015 Antimony sulfide as a light absorber in highly ordered, coaxial nanocylindrical arrays: preparation and integration into a photovoltaic device *J. Mater. Chem. A* **3** 5971
- [21] Gavrilov S, Dronov A, Shevyakov V, Belov A and Poltoratskii E 2009 Ways to Increase the efficiency of solar cells with extremely thin absorption layers *Nanotech. Russia* **4** 237
- [22] Itzhaik Y, O Niitsoo O, Page M and Hodes G 2009 Sb₂S₃-sensitized nanoporous TiO₂ solar cells *J. Phys. Chem. C* **113** 4254
- [23] Senthil T S, Thambidurai M, Muthukumarasamy N and Balasundaraprabhu R 2009 Structural investigations on nanocrystalline TiO₂ thin films prepared by sol-gel spin coating technique *Int. J. Nanosci.* **9** 355
- [24] Yu H F and Wen C W 2011 Photocatalysis and characterization of the gel-derived TiO₂ and P-TiO₂ transparent thin films *Thin Solids Films* **519** 6453
- [25] Manthina V, Correa-Baena J P, Liu G and Agrios A G 2012 ZnO-TiO₂ nanocomposite films for high light harvesting efficiency and fast electron transport in dye-sensitized solar cells *J. Phys. Chem. C* **116** 23864
- [26] Wang S H, Wang K H, Dai Y M and Jehng J M 2013 Water effect on the surface morphology of TiO₂ thin film modified by polyethylene glycol *Appl. Surf. Sci.* **264** 470
- [27] Ito S, Chen P, Comte P, Khaja M, Liska P, Pechy P and Grätzel M 2007 Fabrication of screen printing pastes from TiO₂ powders for dye sensitized solar cells *Prog. Photovoltaics Res. Appl.* **15** 603
- [28] Zhang Y, Zhibin X and Wang J 2010 Pre-curing of supramolecular-templated mesoporous TiO₂ films for dye sensitized solar cells *Thin Solid Films* **518** 34
- [29] Könenkamp R, Ernst K, Fisher C, M Lux-Steiner M and Rost C 2000 Semiconductor growth and junction formation within nanoporous oxides *Phys. Status Solidi. A* **182** 151
- [30] Salazar R, Delamoreanu A, Lévy-Clément C and Ivanova V 2011 ZnO/CdTe and ZnO/CdS core-shell nanowire arrays for extremely thin absorber solar cells *Energy Procedia* **10** 122
- [31] Serpone N, Lawless D and Khairutdinov R 1995 Size effects on the photophysical properties of colloidal anatase TiO₂ particles: size quantization or direct transitions in this indirect semiconductor *J. Phys. Chem.* **99** 16646
- [32] Park N, Lagemaat J and Frank A 2000 Comparison of dye-sensitized rutile and anatase based TiO₂ solar cells *J. Phys. Chem. B* **104** 8989
- [33] Baneree S, Gopal J, Muraleedharan P, Tyagi A K and Raj B 2006 Physics and chemistry of photocatalytic titanium dioxide: visualization of bactericidal activity using atomic force microscopy *Curr. Sci.* **90** 1378
- [34] Ahirrao P B, Gosavi S R, Sonawane S S and Patil R S 2011 Wide band gap nanocrystalline CuSCN thin films deposited by modified chemical method *Arch. Phys. Res.* **2** 29
- [35] Reeja-Jayan B and Manthiram A 2013 Effects of bifunctional metal sulfide interlayers on photovoltaic properties of organic-inorganic hybrid solar cells *RSC Adv.* **3** 5412